Chemical Engineering Journal 390 (2020) 124481

Contents lists available at ScienceDirect

Chemical Engineering Journal

journal homepage: www.elsevier.com/locate/cej

High-performance of Cu-TiO_2 for photocatalytic oxidation of formaldehyde under visible light and the mechanism study

Min Chen[a], Honghong Wang[a], Xueyan Chen[a,b], Fei Wang[a,b], Xiaoxiao Qin[a,b], Changbin Zhang[a,b,*], Hong He[a,b]

[a] State Key Joint Laboratory of Environment Simulation and Pollution Control, Research Center for Eco-Environmental Sciences, Chinese Academy of Sciences, Beijing 100085, China
[b] University of Chinese Academy of Sciences, Beijing 100049, China

HIGHLIGHTS

- Cu-TiO_2 has superior activity for photocatalytic oxidation of HCHO under visible light.
- The presence of H_2O greatly promote the activity for HCHO oxidation.
- CuO_x clusters on TiO_2 have the super reversibility between Cu (II) and Cu (I).
- $^{\cdot}OH$ plays the crucial role in surface formate decomposition rather than the $^{\cdot}O_2^-$.

GRAPHICAL ABSTRACT

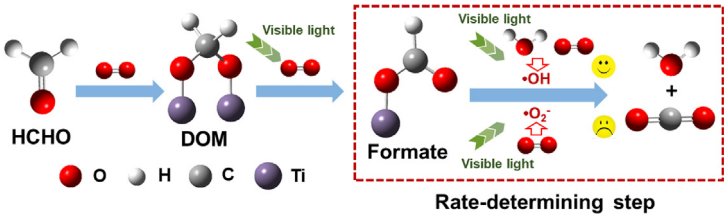

ARTICLE INFO

Keywords:
Photocatalysis
Cu-TiO_2
Formaldehyde
Visible-light

ABSTRACT

Photocatalysis is regarded as a promising method for indoor formaldehyde (HCHO) removal, and there remains a strong demand for the development of highly efficient photocatalysts for HCHO oxidation under visible light. Herein, by grafting nano CuO_x clusters onto TiO_2, the higher performance is achieved over Cu-TiO_2 for the photocatalytic oxidation of HCHO under visible light compared with the typical photocatalysts N-TiO_2 and g-C_3N_4. It is found that the presence of water greatly promotes the activity of HCHO oxidation on Cu-TiO_2. The characterization results indicate that the CuO_x clusters on TiO_2 exhibit high redox reversibility between Cu (II) and Cu (I) and greatly facilitate the migration of electrons. The mechanism of photocatalytic oxidation of HCHO was explored by using *in situ* DRIFTS measurements and DFT calculations. It is shown that HCHO is firstly oxidized to dioxymethylene (DOM), and then DOM is transformed into formate species under visible light irradiation. DFT calculations results indicate that the $^{\cdot}OH$ species are responsible for surface formate decomposition, which is the rate-determining step, while $^{\cdot}O_2^-$ radical is not active in formate decomposition. Our findings improve the understanding on the photocatalytic oxidation of HCHO, and the Cu-TiO_2 catalyst is a promising candidate for practical application in indoor air purification.

1. Introduction

Formaldehyde (HCHO) is one of the most prevalent and noxious indoor gaseous pollutants, and its emission in dwellings mainly stems from the use of inferior decorative materials [1,2]. HCHO is harmful to human health, and long-term exposure to excessive HCHO in the environment even causes cancer. To eliminate HCHO from indoor air, several techniques such as physical adsorption, plasma catalytic

* Corresponding author at: State Key Joint Laboratory of Environment Simulation and Pollution Control, Research Center for Eco-Environmental Sciences, Chinese Academy of Sciences, Beijing 100085, China.
E-mail address: cbzhang@rcees.ac.cn (C. Zhang).

https://doi.org/10.1016/j.cej.2020.124481
Received 14 November 2019; Received in revised form 13 February 2020; Accepted 16 February 2020
Available online 17 February 2020
1385-8947/

oxidation, and thermal catalytic oxidation have been intensively studied [3]. Adsorption materials usually have limited capacities. Plasma may generate harmful byproducts during the elimination of indoor gaseous pollutants. In thermal catalytic oxidation, supported noble metals, including Pt, Pd, and Au, have been reported as highly active catalysts for HCHO removal at ambient temperature [4–7]. However, the high price of noble metals greatly limits their wide application. Non-precious metal oxides, such as MnO_2, still show poor activity under ambient conditions, and thus are not suitable for indoor air HCHO elimination [8,9]. Therefore, it is highly desirable to develop low-cost catalytic materials and/or new methods with high efficiency for HCHO removal at room temperature.

Photocatalysis is currently regarded as an emerging and promising technology for degradation of indoor organic pollutants, such as toluene and acetone or other VOCs [10–17]. By applying an active photocatalyst under UV or visible irradiation, most indoor air pollutants can be well eliminated. TiO_2 is the benchmark photocatalyst and has many advantages, such as strong photocatalytic oxidation, room temperature activity, and photostability [18,19]. With its high energy band gap (ca. 3.0 eV for rutile and 3.2 eV for anatase), the application of TiO_2 is in need of ultraviolet light. Since UV light, especially UV-C light, is directly harmful to the human body, it is not suitable for the elimination of indoor air pollutants. Therefore, there remains a strong demand for the development of visible light responsive photocatalysts for indoor HCHO removal.

Immense efforts have been devoted to extending the photoactivity of TiO_2 into the visible range. Doping the TiO_2 lattice with anions (C, N, etc.) has been shown to introduce impurity states or to narrow the band gap for visible light absorption [20–25]. It was reported that HCHO was photo-degraded over N-doped or N/Ni-co-doped TiO_2 [23,26] N-doped ZnO synthesized by a facile process was also employed to eliminate HCHO, as reported by Wu et al. [27]. Recently, Zhu et al. found that plasmonic Au/TiO_2 exhibited excellent HCHO oxidation activity under visible light, which originated from the cooperation of plasmonically excited photogenerated electrons on Au and surface-active oxygen species [28]. Song et al. showed that the novel material g-C_3N_4 has activity for the photocatalytic oxidation of HCHO [29]. However, there is still a great need for the development of facile and efficient visible-light photocatalysts for application in indoor air purification.

Recently, the grafting of clusters of transition metals, such as Cu, Fe, Ni and Ag, onto TiO_2 was found to induce visible light absorption [30–34]. It was reported that the interfacial charge transfer (IFCT) process occurred under visible light when these metal clusters were grafted on TiO_2 [35–39]. Considering the excellent activity of transition metal-modified TiO_2 in the decomposition of dyes, it is worth exploring whether these catalysts are also highly efficient for the photocatalytic oxidation of HCHO under visible light, and there is no related study to date. Furthermore, the mechanism of photocatalytic oxidation of HCHO has not been fully elucidated. Sun et al. found that $^{\cdot}O_2^-$ and $^{\cdot}OH$ play dominant roles in the formation of formate, which is the main intermediate product [40], and Zhu et al. recently reported that moisture accelerates the oxidation of dioxymethylene (DOM) species to formate; however, the formate decomposition process was not considered [28]. Besides, the roles of $^{\cdot}O_2^-$ and $^{\cdot}OH$ in the photocatalytic oxidation of organic pollutants are the subject of debate. Some researchers hold that $^{\cdot}O_2^-$ plays the critical role, while others contend that $^{\cdot}OH$ dominates in organic pollutant oxidation [41–45]. Thus, from the point of view of reactive intermediates and active species, it is crucially important to gain further insights into the mechanism of the photocatalytic oxidation of HCHO.

In the present study, CuO_x clusters grafted onto TiO_2 catalysts were prepared and their performances in the photocatalytic oxidation of HCHO under visible light were tested. The Cu-TiO_2 catalysts were next characterized by XRD, BET, XPS, EPR, etc., to investigate the structure-function relationship. Finally, the roles of O_2 and H_2O in the HCHO oxidation on Cu-TiO_2 were further investigated by using *in situ* DRIFTS and DFT calculations.

2. Experiment

2.1. Synthesis of catalysts

TiO_2 was purchased from Aladdin, and Cu-TiO_2 was prepared by the impregnation method. 1.0 g TiO_2 was dispersed in a $CuSO_4$ aqueous solution (50 mL), in which the amount of Cu^{2+} relative to the amount of TiO_2 sample was 0.5 wt%. The resulting solution was placed into a water-bath kept at 90 °C for 1 h under stirring. The solid product was washed with deionized water several times and then dried in an oven at 70 °C for 24 h. Graphitic carbon nitride (g-C_3N_4) was synthesized by heating melamine at 550 °C for 4 h. N-TiO_2 was prepared via a sol-gel method [46], wherein tetrabutyl titanate was mixed with a 0.1 M NH_4Cl solution, and the gels obtained subsequently dried at 373 K and finally calcined in air at 673 K for 4 h.

2.2. HCHO oxidation activity test

Activity tests for HCHO oxidation were performed at ambient temperature in a home-made flow reactor. The details of testing setup and the reactor are given in Figs. S1 and S2. 0.1 g of photocatalyst powder was first dispersed in 2 mL deionized water and then placed in a round stainless steel dish with diameter 80 mm, then dried naturally at room temperature, and finally was placed in the center of the reactor. A 500 W commercial Xe lamp (Beijing TrusTech Science and Technology Co., China) was used as the light source with an optical filter ($\lambda > 420$ nm). The light intensity was about 10.2 mW/cm^2. The concentrations of HCHO and CO_2 were measured by an FTIR spectrometer (Nicolet 380) equipped with a 2 m gas cell and a deuterated triglycine sulfate (DTGS) detector. The reactant gas was 250 ppm HCHO, 20 vol% O_2, RH 50% and N_2 balance. For the investigation of RH effect on HCHO conversion, the different RHs (5%, 30%, 60%, 80%) in mixed gases were controlled by changing the flow rate of N_2 bubbling through the water and the temperature of water bath. The volume of reactant gas was about 1.5 L. The gas was driven by a peristaltic pump and the flow rate was around 100 mL/min.

2.3. Characterization

Powder X-ray diffraction (XRD) measurements of the catalysts were carried out on an X'Pert PRO MPD X-ray powder diffractometer (Japan) using Cu Kα radiation operating at 40 kV and 40 mA. The patterns were measured over the 2θ range from 10° to 90° with a scan step size of 0.02°. Transmission electron microscopy (TEM) images of the prepared samples were taken on a JEOL 2100F instrument operating at an accelerating voltage of 200 kV. The UV–vis diffuse reflection spectra (DRS) were obtained in air with Al_2O_3 as reference with a diffuse reflectance UV–vis Spectropho-tometer (U-3310, Hitachi). The structure of the photocatalysts was investigated using X-band electron paramagnetic resonance (EPR) spectra, which were recorded at low temperature (90 K) using a Bruker E500 EPR spectrometer. The photoelectrochemical measurements were conducted on CHI 630B workstation; a slurry of the photocatalyst was spread onto fluorine-doped tin oxide (FTO) glass to prepare the working electrodes. Current-time curves were collected with a 0.1 V bias voltage. The working electrodes were immersed in $NaSO_4$ solution (0.1 M). A saturated Ag/AgCl electrode and a platinum wire were used as the reference electrode and the counter electrode, respectively. In situ DRIFTS spectra were recorded in an IS 50 FTIR equipped with a liquid N_2 cooled MCT detector. The sample (about 30 mg) was finely ground and placed in a ceramic crucible. The flow of feed gas mixture was controlled by mass flow meters. When H_2O was introduced, the RH was adjusted to 50%. All spectra were measured with a resolution of 4 cm^{-1} and accumulation of 100 scans. A background spectrum was subtracted from each

spectrum.

2.4. DFT computational details

The reaction process of $HCOO^-$ and $^{\cdot}OH/O_2$ was investigated by density functional theory (DFT) calculations using the Gaussian 09 program. The structures of neutral Ti_2O_4 clusters, Ti_2O_4-$HCOO^-$ and $^{\cdot}OH/^1O_2$ were optimized at the B3LYP/6-311 G (d, p) level. The H-abstraction of $HCOO^-$ by $^{\cdot}OH$ and $^1O_2$ was examined through relaxed potential energy surface (PES) scans using single internal coordinates. The selected local minima were used as starting equilibrium structures in the scans. For the PES scans in this work, the C—H chemical bond of $HCOO^-$ being evaluated was elongated from the equilibrium bond length 1.1 Å in increments of 0.1 Å. At each step, the relevant bond length was fixed, while the remaining geometric parameters were optimized. The scan results were analyzed to reveal the reaction mechanisms. If there was a saddle point on the scan plot, the geometry corresponding to the saddle point was used for the initial guess structure for the transition state (TS) species optimization. Vibrational frequency calculations were also carried out to check that the IMs and TSs have zero and only one imaginary frequency, respectively. Intrinsic reaction coordinate (IRC) calculations were employed to check that a TS connects two appropriate local minima. The zero-point vibrational corrected energies (ΔH_0) are reported in this work.

3. Results and discussion

3.1. Photocatalytic activity

The synthesized photocatalysts were tested in the photocatalytic oxidation of formaldehyde (PCO of HCHO). For comparison, N-doped TiO_2 and g-C_3N_4 photocatalysts, which are typical visible-light photocatalysts, were used as references. The reaction of HCHO oxidation was negligible when the control experiment was performed under visible irradiation in the absence of photocatalyst. Before the light was turned on, the adsorption of HCHO on the catalyst was allowed to reach equilibrium. Fig. 1a shows the concentration of HCHO versus illumination time over different catalysts under visible light. It is observed that Cu-TiO_2 has excellent activity for the PCO of HCHO, and 100% conversion of 250 ppm HCHO is reached after 140 min reaction under visible light. In contrast, the N-TiO_2 and g-C_3N_4 catalysts have very low activities for HCHO oxidation, and the HCHO conversion levels are 25% and 20%, respectively, after 140 min. The gas products of HCHO oxidation were also examined, and CO_2 was the only gaseous product. As shown in Fig. 1b, the concentration of CO_2 produced on the N-TiO_2 and g-C_3N_4 samples correspond to the concentration of converted HCHO. As for Cu-TiO_2, considering the carbon balance, 250 ppm gaseous HCHO and surface pre-adsorbed HCHO-related species are both oxidized to CO_2, therefore the final detected CO_2 concentrations exceed 250 ppm. It can be deduced that the PCO of HCHO reaction takes place on the surface of Cu-TiO_2, rather than a remote oxidation.

The influence of water vapor on the activity of Cu-TiO_2 was also investigated. Fig. 1c shows a comparison of HCHO conversion levels over Cu-TiO_2 for 140 min visible light illumination under different relative humidity levels. The performance of Cu-TiO_2 is very low when the RH was 5%, and the HCHO conversion is only 40%. With increasing RH from 5% RH to 80% RH, the HCHO conversion is enhanced to 100%. The effects of RH on the performances of N-TiO_2 and g-C_3N_4 were also investigated and the results are shown in Fig. S3. With increasing the RH, the activity of the N-TiO_2 is clearly enhanced, while the activity of the g-C_3N_4 first rise and then fall at 80% RH. It is known that there is usually an optimum RH for the PCO performance, and the rate of PCO reaction will firstly increase then decrease with increasing RH. The negative effect of water vapor on reaction at high RH is mainly attributed to the competitive adsorption of H_2O. However, we do not observe an optimum RH during the PCO of HCHO over Cu-TiO_2, and the H_2O still greatly promotes the HCHO conversion even at 80% RH. Generally, HCHO binds with a Lewis acid site (Ti_{5c}) on metal oxides and then easily reacts with surface active oxygen species to form the dioxymethylene (DOM) species [28]. In contrast, the water adsorption involves a hydrogen bonding interaction with the surface hydroxyl groups of TiO_2 and/or other water molecules. Clearly, HCHO is more strongly adsorbed onto the TiO_2 surface than H_2O molecules. Therefore, the competitive adsorption of H_2O may not be the key factor influencing the photocatalytic oxidation of HCHO, and there should be another key step determining the overall HCHO conversion rate.

3.2. Characterization

The crystallographic structures of the as-synthesized samples were confirmed by XRD measurements. As shown in Fig. 2, Cu-TiO_2 exhibits the standard rutile XRD pattern [JCPDS no. 21-1276, space group: P42/mnm]. No diffraction peaks of Cu or CuO_x appear, indicating that the Cu species are well dispersed on the surface of TiO_2. The N-TiO_2 sample exhibits the standard anatase XRD pattern and g-C_3N_4 shows its typical diffraction peaks at 27.5° and 13.0°, which could be indexed to the (0 0 2) and (1 0 0) planes of graphite-like carbon nitride [45,47]. The BET surface areas of Cu-TiO_2, N-TiO_2 and g-C_3N_4 are measured as about 50, 80 and 14 $m^2 \cdot g^{-1}$ respectively. According to the ICP-OES results, the content of Cu in Cu-TiO_2 is 0.45 wt%. HR-TEM image of the Cu-TiO_2

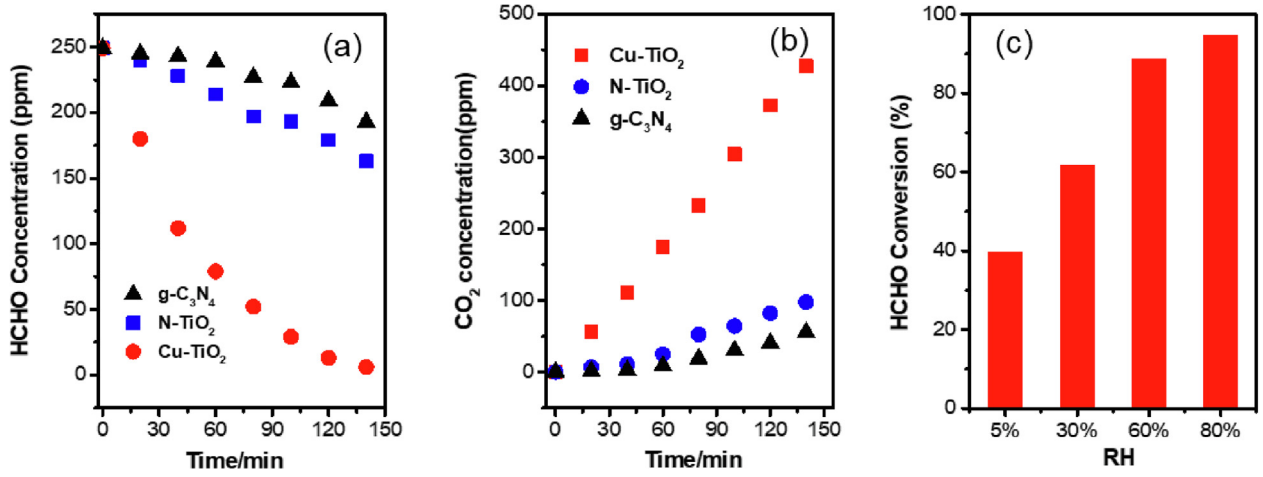

Fig. 1. Photocatalytic oxidation of HCHO: (a) HCHO concentration vs reaction time (b) CO_2 production over Cu-TiO_2, N-TiO_2, g-C_3N_4, and (c) HCHO conversion at different RH over Cu-TiO_2.

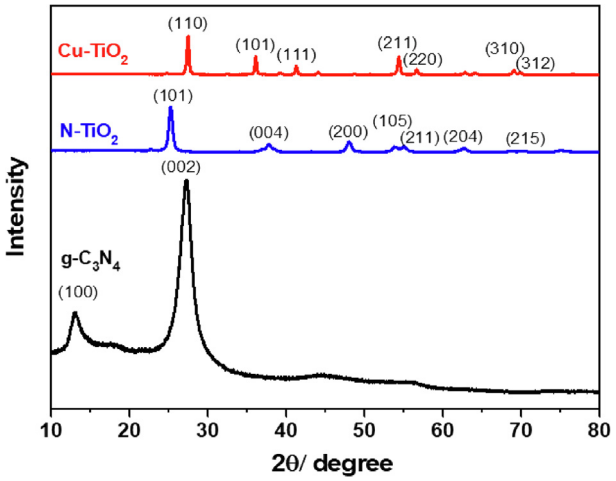

Fig. 2. X-ray diffraction patterns of synthesized samples.

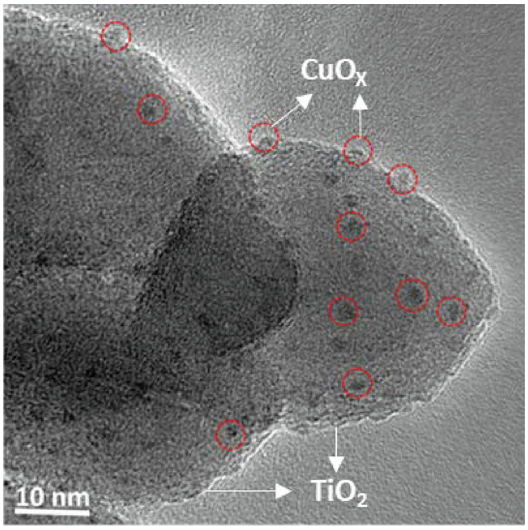

Fig. 3. HR-TEM image of Cu-TiO_2.

sample is presented in Fig. 3. The image shows that the CuO_x clusters are uniformly distributed on the surface of TiO_2, and the size of the CuO_x clusters is approximately 1–2 nm. Previous studies demonstrated that CuO_x clusters attach to the TiO_2 surface via binding of O atoms in the clusters with unsaturated 5c-Ti atoms [48].

XPS analysis was employed to further detect the chemical states of the surface CuO_x on Cu-TiO_2. As shown in Fig. 4a, Cu-TiO_2 exhibits two peaks of Cu $2p_{1/2}$ (952.9 eV) and Cu $2p_{3/2}$ (933.1 eV), respectively, which can be assigned to either Cu^0 or Cu^+ because the binding energies of both states are nearly the same and cannot be discerned by XPS [36,38,49]. Since Cu-TiO_2 was synthesized by a facile impregnation method with copper nitrate and no subsequent reduction, it is unlikely that the CuO_x contained copper in the Cu^0 state. We further conducted an EPR experiment to explore the structure of CuO_x. As shown in Fig. 4b, no EPR signal is detected before grafting of CuO_x species on TiO_2. After CuO_x is loaded on TiO_2, an EPR signal with the g factor of 2.394 appears, and this signal is ascribed to Cu^{2+} species [50]. We also carried out FTIR measurements to investigate the states present in CuO_x by using CO adsorption as a probe, and the results are presented in Fig. S4. An IR band at 2104 cm^{-1} appears after CO adsorption, which is attributed to linearly adsorbed CO species on Cu^+ sites (Cu^+–CO) [49]. These results indicate that Cu^{2+} and Cu^+ species may coexist on the surface of Cu-TiO_2; furthermore, the surface Cu^{2+} are easily reduced to Cu^+ by CO adsorption or by x-ray beam irradiation in the high-vacuum chamber of the XPS instrument. Thus, it is suggested that the Cu species on the surface of Cu-TiO_2 have high redox reversibility between Cu (II) and Cu (I).

Visible light absorption is obviously a crucial precondition for a visible-light-sensitive photocatalyst. The UV–vis diffuse reflectance spectra (DRS) of the samples were measured. As displayed in Fig. 5, the absorption intensity of TiO_2 starts to increase at ~410 nm, corresponding to the band gap of 3.0 eV. In case of Cu-TiO_2, the spectra show absorption in the ~700 − 800 nm region, which can be attributed to the Cu (II) d-d transition, and also a shoulder peak at ~450 nm, which might be due to direct interfacial charge transfer from the VB of TiO_2 to Cu^{2+} species, as reported by Hashimoto et al. [36]. N-TiO_2 and g-C_3N_4 are typical visible-light-sensitive photocatalysts, and used as reference materials here. Fig. S5 shows that N-TiO_2 has a broad absorption in the visible region centered at about 450 nm, which is the characteristic absorption of N-doped TiO_2 [20,21]. The absorption edge of the g-C_3N_4 sample is about 460 nm, which corresponds well with the band gap of pristine g-C_3N_4 (2.7 eV) [47].

The separation of photoexcited charges is the crucial step that determines the photocatalytic efficiency of a photocatalyst. Transient photocurrent is often used to investigate the charge separation efficiency. Fig. 6 displays the photocurrent curves of the samples under visible light. Negligible photocurrent is detected for the pure TiO_2 electrodes owing to their wide band gaps. After grafting with CuO_x nanoclusters, the photocurrent of Cu-TiO_2 noticeably increases. In contrast, the prepared N-TiO_2 and g-C_3N_4 exhibits photocurrents that are clearly lower compared with Cu-TiO_2. Previous studies have reported that the interfacial charge transfer (IFCT) process between TiO_2 and metal oxides can greatly enhance the charge separation [33,37], thus the remarkably increased photocurrent on Cu-TiO_2 under visible light may stem from IFCT. High photocurrent indicates a low rate of recombination of electron-hole pairs, and the photocurrent results agree well with the results of the activity tests, in which Cu-TiO_2 exhibits the higher performance for HCHO oxidation than N-TiO_2 or g-C_3N_4.

The interfacial charge transfer behavior in Cu-TiO_2 was further characterized by electrochemical impedance spectroscopy (EIS). The capacitance arc of the EIS Nyquist plot reveals the conductivity of materials, as well as the charge migration kinetics during the photocatalytic process. As shown in Fig. 7. Cu-TiO_2 exhibits a smaller capacitance arc than that of TiO_2, suggesting that CuO_x clusters can be functional as an electron collector and transporter in Cu-TiO_2, thus facilitating the process of interfacial charge transfer. In combination with the results on the chemical states of CuO_x on Cu-TiO_2 (Fig. 4, Fig. S4), which suggest high redox reversibility between Cu (II) and Cu (I) on the Cu-TiO_2 surface, it is reasonable that the photoexcited electrons are inclined to be captured by Cu (II) and then produce Cu (I) under visible light, and Cu (I) is next rapidly oxidized by O_2 to recover to Cu (II), therefore greatly enhancing the migration of photoexcited electrons.

3.3. Mechanism of the photocatalytic oxidation of HCHO

In order to identify the intermediates in the PCO of HCHO over Cu-TiO_2, a series of in situ DRIFTS experiments was conducted. DRIFTS spectra were measured in the range of 1800–1000 cm^{-1} over Cu-TiO_2 with the introduction of the HCHO and O_2, and the results are shown in Fig. S6. Four peaks quickly appear at 1096, 1147, 1171, and 1407 cm^{-1}, which are all attributed to the dioxymethylene (DOM) species [51]. Meanwhile, formate species (1545, 1358 and 1377 cm^{-1}) for $\nu(COO^-)$ are also formed [52,53], indicating that some DOM are converted into formate species. As shown in Fig. 8, the DOM species rapidly disappear when the visible light is introduced, which is revealed by the disappearance of the peaks at 1096, 1147, and 1171 cm^{-1}. At the same time, the peaks of formate at 1545, 1358 and 1377 cm^{-1} continually increase, indicating that formate species are accumulated

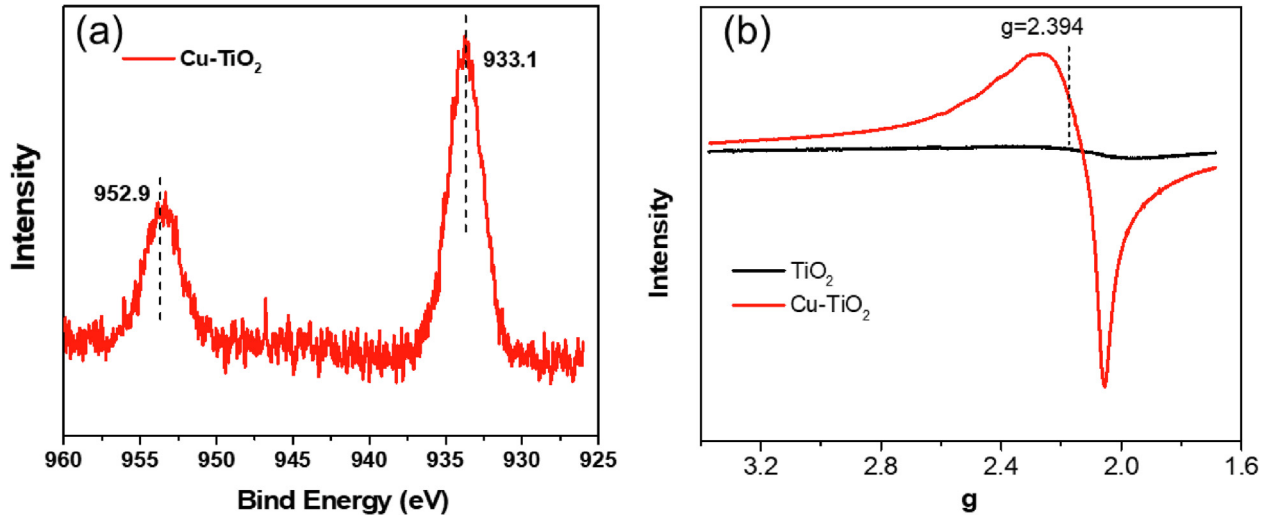

Fig. 4. High resolution Cu 2p XPS spectra (a) and EPR spectra (b) of Cu-TiO_2.

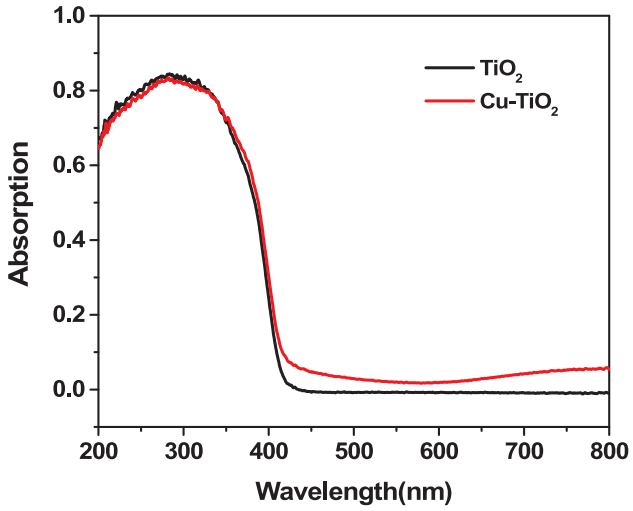

Fig. 5. UV–vis diffuse reflectance spectra of the samples.

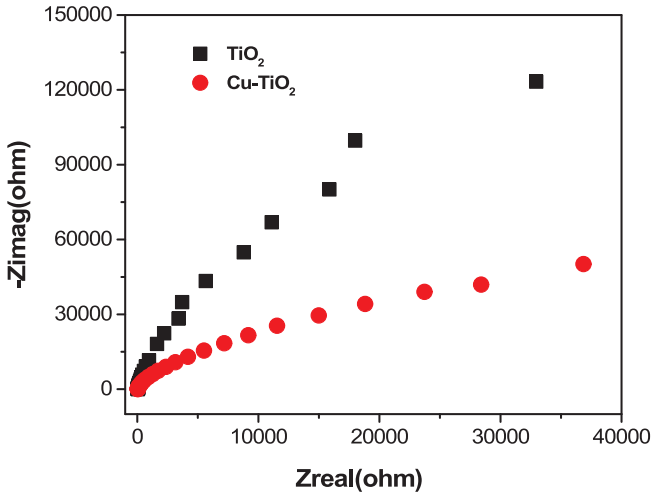

Fig. 7. EIS Nyquist plots of the prepared TiO_2 and Cu-TiO_2 electrodes under visible-light irradiation.

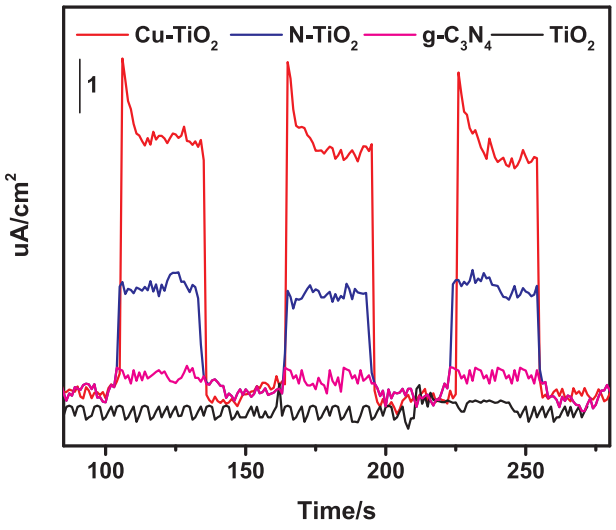

Fig. 6. Photocurrent curves vs time of the samples under visible light.

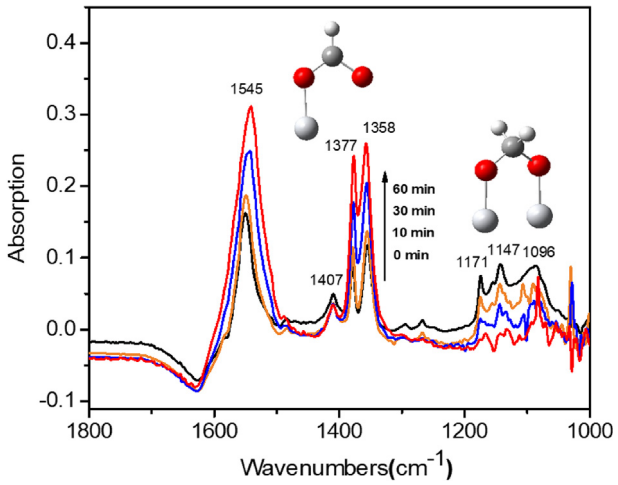

Fig. 8. In situ DRIFTS spectra over Cu-TiO_2 in a flow of He + HCHO + O_2 under visible light. Reaction conditions: 120 ppm of HCHO, 20% O_2, He balance, total flow rate of 100 cm^3 min^{-1}.

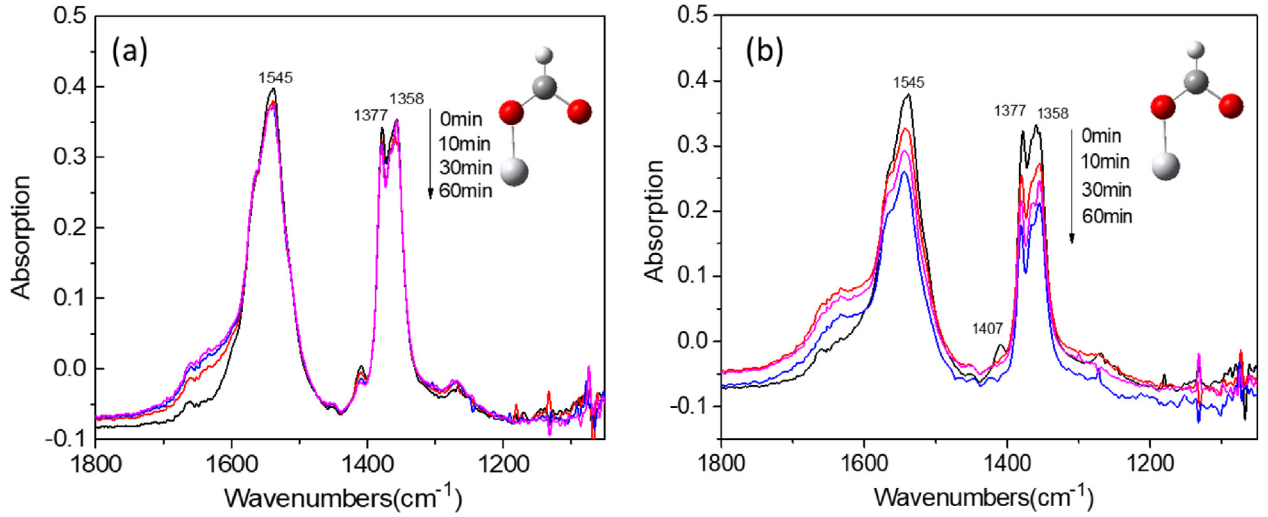

Fig. 9. Dynamic changes of in situ DRIFTS spectra over Cu-TiO_2 after O_2 (a) and O_2 and H_2O (b) purging 20% O_2, 50% RH, He balance, total flow rate of 100 cm^3 min^{-1}.

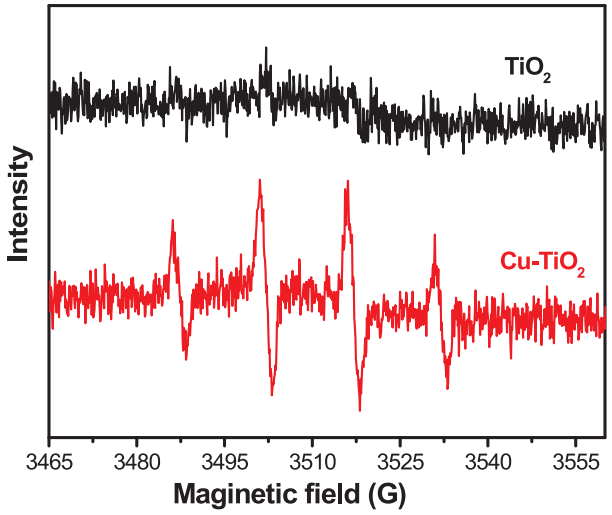

Fig. 10. DMPO spin-trapping EPR spectra after 5 min visible irradiation in aqueous solutions over different samples.

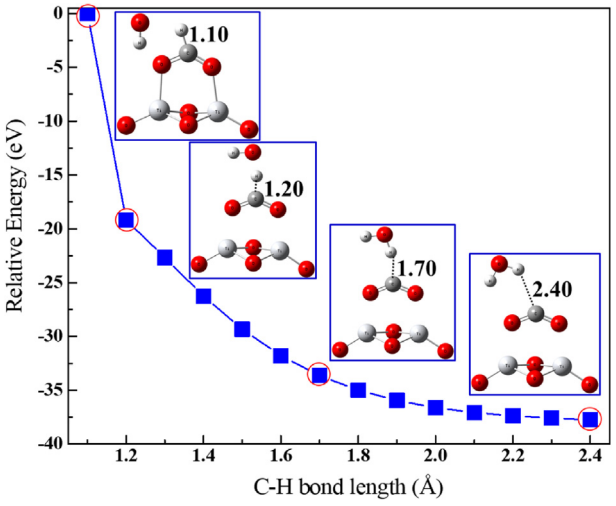

Fig. 11. Potential energy curve for the breaking process of $HCOO^-$ at the B3LYP/6-311 G (d, p) level. The dotted line denotes the relative energy of Ti_2O_4-$HCOO^-$ + $^{\cdot}OH$.

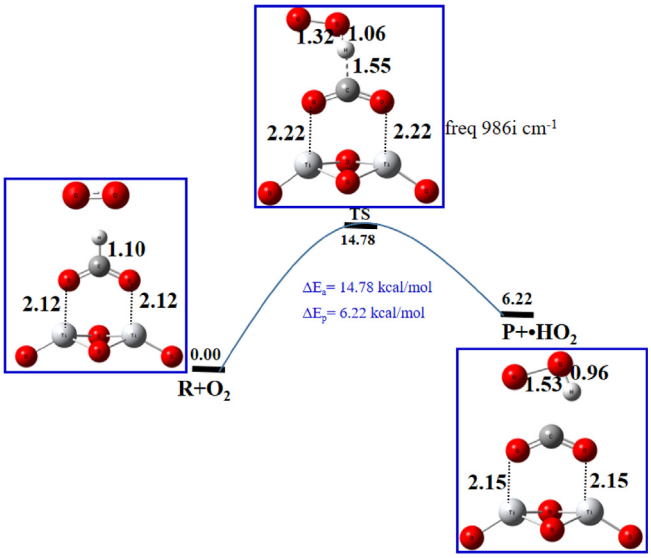

Fig. 12. Potential energy profile for $HCOO^-$ oxidation by $^1O_2$, the bond length and the relative energies are in units of Å and kcal/mol, respectively.

on the surface of Cu-TiO_2. It is suggested that DOM is oxidized to formate species in the photocatalytic oxidation of HCHO. The flow of HCHO and O_2 are next switched to O_2 only. As shown in Fig. 9a, no obvious changes are observed in the spectra after 60 min exposure to O_2 under visible light, indicating that the adsorbed formate species remain very stable toward O_2 under visible light irradiation. H_2O is next introduced into the flow, as shown in Fig. 9b, a quick decrease in the bands related to formate species is observed in the DRIFTS spectra. Therefore, it is clear that H_2O promotes the process of formate decomposition.

Intermediate reactive oxygen species play a very important role in the photocatalytic oxidation process. In case of the Cu-TiO_2, many researchers have recently reported that holes and electrons are generated due to the interfacial charge transfer process under visible light irradiation [35,54]. When there is no water vapor, the dominant reactive species are the holes and $^{\cdot}O_2^-$ formed by the activation of O_2 by photoexcited electrons, which has been measured by MCLA chemiluminescence by Nosaka et al [54]. We conducted EPR experiments with DMPO as the trapping agent to explore the reactive oxygen species in Cu-TiO_2. As shown in Fig. 10, the characteristic peaks of DMPO-$^{\cdot}$OH

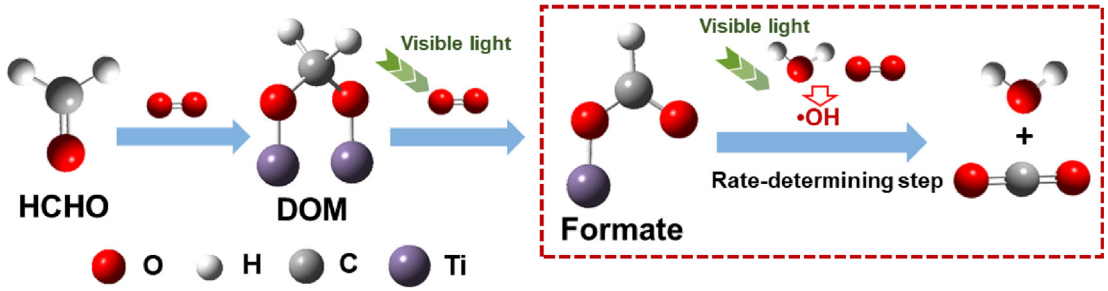

Fig. 13. Schematic illustration of the reaction process for the photocatalytic oxidation of HCHO over Cu-TiO_2.

adducts appear under visible light in Cu-TiO_2, indicating the formation of ˙OH. In contrast, no signals of DMPO-˙OH adducts are observed in the case of TiO_2. Fig. S7 shows that Cu-TiO_2 can also produce $˙O_2^-$ under visible light. These results suggest that when H_2O is available, Cu-TiO_2 produces ˙OH species under visible light, participating in the PCO of HCHO. Since the competitive adsorption of H_2O is not the key factor influencing the PCO of HCHO and the higher RH is favorable for the production of more ˙OH species, the increase of the RH greatly enhances the HCHO conversions even at a high RH of 80%.

To further understand the key active species in the process of formate decomposition in the photocatalytic oxidation of HCHO, a series of DFT calculations were conducted. When ˙OH radicals attack the formate species on TiO_2, the PES scans are carried out to run for a C—H distance from 1.10 to 2.40 Å in 0.1 Å increments. The plot of the PES scan and corresponding structures are shown in Fig. 11. When the C—H distance is 1.10 Å, there is only weak interaction between $HCOO^-$ and ˙OH. The total energy of Ti_2O_4-C (OO)…H-OH decreased from −19.19 to −33.63 kcal/mol, as the C—H bond is elongated from 1.20 to 1.70 Å. The hydrogen of $HCOO^-$ is abstracted by ˙OH when the C—H distance was 1.70 Å. There is no saddle point in the scan plot, which means that no transition state existed in the process of ˙OH attack the $HCOO^-$. In other words, the abstraction of hydrogen from $HCOO^-$ by ˙OH is exothermic (ΔH_0 = -19.06 kcal/mol) and barrierless (Eq. (1–1)). The process of the excited O_2 attacking the formate has also been calculated (Fig. 12). This transfer of hydrogen from $HCOO^-$ to $^1O_2$ has to overcome a barrier of 14.78 kcal/mol, and absorb heat (ΔH_0 = +6.22 kcal/mol) (Eq. (1–2)). These results clearly show that this process is thermodynamically and kinetically unfavorable. In fact, holes and $˙O_2^-$ are the main reactive oxygen species under dry conditions, and the HCHO oxidation activity is very poor. The DRIFTS result also shows that the formate species remain intact in the presence of O_2, showing that $˙O_2^-$ is not the main active species in HCHO oxidation. When H_2O is introduced into the flow, the main reactive oxygen species are changed to holes, $˙O_2^-$ and ˙OH, and the activity is greatly enhanced. Thus, the theoretical calculations strongly support and interpret the experimental observation that ˙OH plays an important role in promoting photocatalytic HCHO oxidation.

$$Ti_2O_4\text{-}HCOO^- + OH \rightarrow Ti_2O_4\text{-}CO_2 + H_2O\ \Delta H_0 = -19.06\ \text{kcal/mol} \quad (1\text{–}1)$$

$$Ti_2O_4\text{-}HCOO^- + {}^1O_2 \rightarrow Ti_2O_4\text{-}CO_2 + HO_2^-\ \Delta H_0 = +6.22\ \text{kcal/mol} \quad (1\text{–}2)$$

Based on the above results, we deduced that HCHO oxidation undergoes a series of sequential reaction steps. As shown in Fig. 13, HCHO is firstly adsorbed on the surface of Cu-TiO_2, and CH_2O_2 is quickly formed because the HCHO is easily oxidized by surface-active oxygen or hydroxyl. CH_2O_2 is not a stable intermediate species and is further transformed to the stable formate species. This process even takes place under dark conditions, and is greatly enhanced when visible light excites the Cu-TiO_2, in which the active holes and $˙O_2^-$ play significant roles. Formate decomposition as the rate-determining step in the catalytic oxidation of HCHO has been extensively reported [52,55]. Formate is decomposed by reacting with surface hydroxyls activated by Pt or Pd metals, and directly converted to CO_2 and H_2O; this path is preferred over the decomposition of formate to CO followed by CO oxidation [52]. In our present studies, when the flow is H_2O-free, the formate species are hardly decomposed, resulting in overall poor HCHO activity. However, under moist conditions, the formate is gradually decomposed, therefore leading to an enhanced HCHO conversion. Previous studies have reported that $˙O_2^-$ plays the critical role in the oxidation of many organic pollutants, in which the scission of C—C bonds is realized by inserting the oxygen of O_2 into the C—C bonds [56,57]. However, $˙O_2^-$ is not the active species in the dehydrogenation process of formate species to form CO_2. It should be noted that even through $˙O_2^-$ does not directly participate in the decomposition of formate, $˙O_2^-$ is able to produce ˙OH by reacting with H_2O. Hence, it can be inferred that ˙OH dominates the dehydrogenation step in organic pollutant oxidation.

4. Conclusions

In summary, we constructed a Cu-TiO_2 catalyst with nano CuO_x clusters grafted onto TiO_2. The Cu-TiO_2 catalyst demonstrates much higher performance than N-TiO_2 or g-C_3N_4 for the PCO of HCHO, reaching 100% HCHO conversion to CO_2 within 140 min. The CuO_x clusters on TiO_2 exhibit high redox reversibility between Cu (II) and Cu (I) and greatly facilitate the separation of holes and electrons. The presence of H_2O greatly promotes the activity for HCHO oxidation, and *in situ* DRIFTS and DFT calculations results confirm that ˙OH radical plays the crucial role in surface formate decomposition, rather than $˙O_2^-$. These findings will deepen our understanding of the photocatalytic oxidation of organic contaminates.

Declaration of competing interest

The authors declare that they have no known competing financial interests or personal relationships that could have appeared to influence the work reported in this paper.

Acknowledgements

This work was financially supported by the National Key R&D Program of China (2017YFC0211802) and the National Natural Science Foundation of China (21906174, 21976196) and China Postdoctoral Science Foundation (2018M641494).

Appendix A. Supplementary data

Supplementary data to this article can be found online at https://doi.org/10.1016/j.cej.2020.124481.

References.

[1] X.J. Tang, Y. Bai, A. Duong, M.T. Smith, L.Y. Li, L.P. Zhang, Formaldehyde in China: production, consumption, exposure levels, and health effects, Environ. Int. 35

(2010) 1210–1224.
[2] R. Maddalena, M. Russell, D.P. Sullivan, M.G. Apte, Formaldehyde and other volatile organic chemical emissions in four FEMA temporary housing units, Environ. Sci. Technol. 43 (2009) 5626–5632.
[3] J.Q. Torres, S. Royer, J.P. Bellat, J.M. Giraudon, J.F. Lamonier, Formaldehyde: catalytic oxidation as a promising soft way of elimination, ChemSusChem 6 (2013) 578–592.
[4] H. Tan, J. Wang, S. Yu, K. Zhou, Support morphology-dependent catalytic activity of Pd/CeO_2 for formaldehyde oxidation, Environ. Sci. Technol. 49 (2015) 8675–8682.
[5] H.F. Li, N. Zhang, P. Chen, M.F. Luo, J.Q. Lu, High surface area Au/CeO2 catalysts for low temperature formaldehyde oxidation, Appl. Catal., B 110 (2011) 279–285.
[6] C.B. Zhang, H. He, K. Tanaka, Catalytic performance and mechanism of a Pt/TiO_2 catalyst for the oxidation of formaldehyde at room temperature, Appl. Catal., B 65 (2006) 37–43.
[7] C.B. Zhang, H. He, K. Tanaka, Perfect catalytic oxidation of formaldehyde over a Pt/TiO_2 catalyst at room temperature, Catal. Commun. 6 (2005) 211–214.
[8] L. Zhu, J.L. Wang, S.P. Rong, H.Y. Wang, P.Y. Zhang, Cerium modified birnessite-type MnO_2 for gaseous formaldehyde oxidation at low temperature, Appl. Catal., B 211 (2017) 212–221.
[9] J.H. Zhang, Y.B. Li, L. Wang, C.B. Zhang, H. He, Catalytic oxidation of formaldehyde over manganese oxides with different crystal structures, Catal. Sci. Technol. 5 (2015) 2305–2313.
[10] A. Fujishima, X.T. Zhang, D.A. Tryk, TiO_2 photocatalysis and related surface phenomena, Surf. Sci. Rep. 63 (2008) 515–582.
[11] M.R. Hoffmann, S.T. Martin, W.Y. Choi, D.W. Bahnemann, Environmental applications of semiconductor photocatalysis, Chem. Rev. 95 (1995) 69–96.
[12] L. Zhong, J.J. Brancho, S. Batterman, B.M. Bartlett, C. Godwin, Experimental and modeling study of visible light responsive photocatalytic oxidation (PCO) materials for toluene degradation, Appl. Catal., B 216 (2017) 122–132.
[13] J. Mo, Y. Zhang, Q. Xu, J.J. Lamson, R. Zhao, Photocatalytic purification of volatile organic compounds in indoor air: A literature review, Atmos. Environ. 43 (2009) 2229–2246.
[14] L. Zhong, F. Haghighat, Photocatalytic air cleaners and materials technologies - Abilities and limitations, Build. Environ. 91 (2015) 191–203.
[15] X.-Q. Deng, X. Zhu, Z.-G. Sun, X.-S. Li, J.-L. Liu, C. Shi, A.-M. Zhu, Exceptional activity for photocatalytic mineralization of formaldehyde over amorphous titania nanofilms, Chem. Eng. J. 306 (2016) 1001–1009.
[16] Z. Shayegan, C.-S. Lee, F. Haghighat, TiO_2 photocatalyst for removal of volatile organic compounds in gas phase – A review, Chem. Eng. J. 334 (2018) 2408–2439.
[17] S.C. Pillai, U.L. Stangar, J.A. Byrne, A. Perez-Larios, D.D. Dionysiou, Photocatalysis for disinfection and removal of contaminants of emerging concern, Chem. Eng. J. 261 (2015) 1–2.
[18] J. Low, B. Cheng, J. Yu, Surface modification and enhanced photocatalytic CO_2 reduction performance of TiO_2: a review, Appl. Surf. Sci. 392 (2017) 658–686.
[19] G. Liu, H.G. Yang, J. Pan, Y.Q. Yang, G.Q. Lu, H.M. Cheng, Titanium Dioxide Crystals with Tailored Facets, Chem. Rev. 114 (2014) 9559–9612.
[20] R. Asahi, T. Morikawa, T. Ohwaki, K. Aoki, Y. Taga, Visible-light photocatalysis in nitrogen-doped titanium oxides, Science 293 (2001) 269–271.
[21] R. Asahi, T. Morikawa, H. Irie, T. Ohwaki, Visible-light photocatalysis in nitrogen-doped titanium oxides, Chem. Rev. 114 (2014) 9824–9852.
[22] J.H. Park, S. Kim, A.J. Bard, Novel carbon-doped TiO_2 nanotube arrays with high aspect ratios for efficient solar water splitting, Nano Lett. 6 (2006) 24–28.
[23] Z. Han, V.-W. Chang, X. Wang, T.-T. Lim, L. Hildemann, Experimental study on visible-light induced photocatalytic oxidation of gaseous formaldehyde by polyester fiber supported photocatalysts, Chem. Eng. J. 218 (2013) 9–18.
[24] M. Pelaez, N.T. Nolan, S.C. Pillai, M.K. Seery, P. Falaras, A.G. Kontos, P.S.M. Dunlop, J.W.J. Hamilton, J.A. Byrne, K. O'Shea, M.H. Entezari, D.D. Dionysiou, A review on the visible light active titanium dioxide photocatalysts for environmental applications, Appl. Catal., B 125 (2012) 331–349.
[25] L. Xu, X. Bai, L. Guo, S. Yang, P. Jin, L. Yang, Facial fabrication of carbon quantum dots (CDs)-modified N-TiO_{2-x} nanocomposite for the efficient photoreduction of Cr (VI) under visible light, Chem. Eng. J. 357 (2019) 473–486.
[26] X. Zhang, Q. Liu, Visible-light-induced degradation of formaldehyde over titania photocatalyst co-doped with nitrogen and nickel, Appl. Surf. Sci. 254 (2008) 4780–4785.
[27] C. Wu, Facile one-step synthesis of N-doped ZnO micropolyhedrons for efficient photocatalytic degradation of formaldehyde under visible-light irradiation, Appl. Surf. Sci. 319 (2014) 237–243.
[28] X.B. Zhu, C. Jin, X.S. Li, J.L. Liu, Z.G. Sun, C. Shi, X.G. Li, A.M. Zhu, Photocatalytic formaldehyde oxidation over plasmonic Au/TiO_2 under visible light: moisture indispensability and light enhancement, ACS Catal. 7 (2017) 6514–6524.
[29] S. Song, C. Lu, X. Wu, S. Jiang, C. Sun, Z. Le, Strong base g-C_3N_4 with perfect structure for photocatalytically eliminating formaldehyde under visible-light irradiation, Appl. Catal., B 227 (2018) 145–152.
[30] H. Zhang, W. Wang, H. Zhao, L. Zhao, L.-Y. Gan, L.-H. Guo, Facet-dependent interfacial charge transfer in Fe (III)-grafted TiO_2 nanostructures activated by visible light, ACS Catal. 8 (2018) 9399–9407.
[31] M. Liu, X. Qiu, M. Miyauchi, K. Hashimoto, Energy-level matching of Fe(III) ions grafted at surface and doped in bulk for efficient visible-light photocatalysts, J. Am. Chem. Soc. 135 (2013) 10064–10072.
[32] K. Osako, K. Matsuzaki, T. Susaki, S. Ueda, G. Yin, A. Yamaguchi, H. Hosono, M. Miyauchi, Direct observation of interfacial charge transfer between rutile TiO_2 and ultrathin CuO_x film by visible-light illumination and its application for efficient photocatalysis, ChemCatChem 10 (2018) 3666–3670.
[33] A. Iwaszuk, M. Nolan, Q. Jin, M. Fujishima, H. Tada, Origin of the visible-light response of nickel(II) oxide cluster surface modified titanium(IV) dioxide, J. Phys. Chem. C 117 (2013) 2709–2718.
[34] S. Zhao, J. Chen, Y. Liu, Y. Jiang, C. Jiang, Z. Yin, Y. Xiao, S. Cao, Silver nanoparticles confined in shell-in-shell hollow TiO_2 manifesting efficiently photocatalytic activity and stability, Chem. Eng. J. 367 (2019) 249–259.
[35] M. Miyauchi, H. Irie, M. Liu, X. Qiu, H. Yu, K. Sunada, K. Hashimoto, Visible-light-sensitive photocatalysts: nanocluster-grafted titanium dioxide for indoor environmental remediation, J. Phys. Chem. Lett. 7 (2016) 75–84.
[36] H. Irie, K. Kamiya, T. Shibanuma, S. Miura, D.A. Tryk, T. Yokoyama, K. Hashimoto, Visible light-sensitive Cu(II)-grafted TiO_2 photocatalysts: activities and x-ray absorption fine structure analyses, J. Phys. Chem. C 113 (2009) 10761–10766.
[37] A. Suligoj, I. Arcon, M. Mazaj, G. Drazic, D. Arcon, P. Cool, U.L. Stangar, N.N. Tusar, Surface modified titanium dioxide using transition metals: nickel as a winning transition metal for solar light photocatalysis, J. Mat. Chem. A. 6 (2018) 9882–9892.
[38] B.-H. Lee, S. Park, M. Kim, A.K. Sinha, S.C. Lee, E. Jung, W.J. Chang, K.-S. Lee, J.H. Kim, S.-P. Cho, H. Kim, K.T. Nam, T. Hyeon, Reversible and cooperative photoactivation of single-atom Cu/TiO_2 photocatalysts, Nat. Mater. 18 (2019) 620–626.
[39] W. Mulewa, M. Tahir, N.A.S. Amin, MMT-supported Ni/TiO_2 nanocomposite for low temperature ethanol steam reforming toward hydrogen production, Chem. Eng. J. 326 (2017) 956–969.
[40] S. Sun, J. Ding, J. Bao, C. Gao, Z. Qi, C. Li, Photocatalytic oxidation of gaseous formaldehyde on TiO_2: An in situ DRIFTS study, Cat. Let. 137 (2010) 239–246.
[41] X.B. Pang, W. Chang, C.C. Chen, H.W. Ji, W.H. Ma, J.C. Zhao, Determining the TiO_2-photocatalytic aryl-ring-opening mechanism in aqueous solution using oxygen-18 labeled O_2 and H_2O, J. Am. Chem. Soc. 136 (2014) 8714–8721.
[42] C.C. Chen, W.H. Ma, J.C. Zhao, Semiconductor-mediated photodegradation of pollutants under visible-light irradiation, Chem. Soc. Rev. 39 (2010) 4206–4219.
[43] W. Liu, Y. Gao, Y. Yang, Q. Zou, G. Yang, Z. Zhang, H. Li, Y. Miao, H. Li, Y. Huo, Photocatalytic composite of a floating BiOBr@graphene oxide@melamine foam for efficient removal of organics, ChemCatChem 10 (2018) 2394–2400.
[44] Y. Wang, L. Zhang, K. Deng, X. Chen, Z. Zou, Low temperature synthesis and photocatalytic activity of rutile TiO_2 nanorod superstructures, J. Phys. Chem. C 111 (2007) 2709–2714.
[45] D. Zhang, Y.L. Guo, Z.K. Zhao, Porous defect-modified graphitic carbon nitride via a facile one-step approach with significantly enhanced photocatalytic hydrogen evolution under visible light irradiation, Appl. Catal., B 226 (2018) 1–9.
[46] M. Ceotto, L. Lo Presti, G. Cappelletti, D. Meroni, F. Spadavecchia, R. Zecca, M. Leoni, P. Scardi, C.L. Bianchi, S. Ardizzone, About the nitrogen location in nanocrystalline N-doped TiO_2: combined DFT and EXAFS approach, J. Phys. Chem. C 116 (2012) 1764–1771.
[47] J. Yu, S. Wang, J. Low, W. Xiao, Enhanced photocatalytic performance of direct Z-scheme g-C_3N_4-TiO_2 photocatalysts for the decomposition of formaldehyde in air, Phys. Chem. Chem. Phys. 15 (2013) 16883–16890.
[48] M.V. Dozzi, G.L. Chiarello, M. Pedroni, S. Livraghi, E. Giamello, E. Selli, High photocatalytic hydrogen production on Cu(II) pre-grafted Pt/TiO_2, Appl. Catal., B 209 (2017) 417–428.
[49] A. Chen, X. Yu, Y. Zhou, S. Miao, Y. Li, S. Kuld, J. Sehested, J. Liu, T. Aoki, S. Hong, M.F. Camellone, S. Fabris, J. Ning, C. Jin, C. Yang, A. Nefedov, C. Woell, Y. Wang, W. Shen, Structure of the catalytically active copper-ceria interfacial perimeter, Nat. Catal. 2 (2019) 334–341.
[50] Y.J. Kim, J.K. Lee, K.M. Min, S.B. Hong, I.-S. Nam, B.K. Cho, Hydrothermal stability of Cu-SSZ13 for reducing NO_x by NH_3, J. Catal. 311 (2014) 447–457.
[51] T. Kecskés, J. Raskó, J. Kiss, FTIR and mass spectrometric studies on the interaction of formaldehyde with TiO_2 supported Pt and Au catalysts, Appl. Catal., A 273 (2004) 55–62.
[52] C. Zhang, F. Liu, Y. Zhai, H. Ariga, N. Yi, Y. Liu, K. Asakura, M. Flytzani-Stephanopoulos, H. He, Alkali-Metal-Promoted Pt/TiO_2 opens a more efficient pathway to formaldehyde oxidation at ambient temperatures, Angew. Chem., Int. Ed. 51 (2012) 9628–9632.
[53] Y.B. Li, C.B. Zhang, J.Z. Ma, M. Chen, H. Deng, H. He, High temperature reduction dramatically promotes Pd/TiO_2 catalyst for ambient formaldehyde oxidation, Appl. Catal., B 217 (2017) 560–569.
[54] Y. Nosaka, S. Takahashi, H. Sakamoto, A.Y. Nosaka, Reaction mechanism of Cu(II)-grafted visible-light responsive TiO_2 and WO_3 photocatalysts studied by means of ESR spectroscopy and chemiluminescence photometry, J. Phys. Chem. C 115 (2011) 21283–21290.
[55] C.B. Zhang, Y.B. Li, Y.F. Wang, H. He, Sodium-promoted Pd/TiO_2 for catalytic oxidation of formaldehyde at ambient temperature, Environ. Sci. Technol. 48 (2014) 5816–5822.
[56] H. Sheng, Q. Li, W.H. Ma, H.W. Ji, C.C. Chen, J.C. Zhao, Photocatalytic degradation of organic pollutants on surface anionized TiO_2: Common effect of anions for high hole-availability by water, Appl. Catal., B 138 (2013) 212–218.
[57] T. Shi, W. Chang, H.N. Zhang, H.W. Ji, W.H. Ma, C.C. Chen, J.C. Zhao, H_2O-involved two-electron pathway for photooxidation of aldehydes on TiO_2: An isotope labeling Study, Environ. Sci. Technol. 49 (2015) 3024–3031.